Modular Platform Layout Design for a Range-Extended Electric Vehicle (REEV) Chassis

Rohan Joshi and Rudraksh Sharma

IIT Bombay and IIT Kharagpur

Abstract

Range-Extended Electric Vehicles (REEVs) combine a complete battery-electric drivetrain with an internal combustion engine (ICE) and generator to extend usable range beyond what pure battery capacity permits. This paper presents a modular platform layout methodology for a REEV chassis and validates each stage of that methodology against independent data or a second modeling approach. Specifically, we develop and cross-validate: (1) A two-stage spreadsheet-to-WLTC-drive-cycle powertrain sizing pipeline, benchmarked against three production REEVs; (2) A coupled ANSYS/1D-analytical exhaust thermal model; (3) A mass/inertia-matrix modal analysis tool validated against ANSYS FEA; and (4) An AIS-to-international standards equivalency mapping tool used to conduct a structured homologation review. Using this methodology, three candidate chassis layouts: Front-wheel drive (FWD), Rear-wheel drive (RWD), and All-wheel drive (AWD) were developed in CAD and evaluated against packaging, thermal, weight-distribution, and cost criteria. The selected RWD-biased layout achieves a pure EV range of 200 km and a total extended range of 1546 km with a 45 kWh LFP battery, a 1.5 L turbocharged four-cylinder engine, and a 250 kW traction motor, meeting AIS thermal and structural safety limits after the introduction of heat shielding around the fuel tank and battery pack. We additionally propose an offline dynamic-programming (DP) / online neural-network (NN) energy management architecture, for which literature-informed projections suggest a 7–10% fuel-economy improvement over a conventional charge-depleting/charge-sustaining (CD/CS) baseline; this component is explicitly future work.

Keywords—*Range-Extended Electric Vehicle (REEV), Chassis Layout, Powertrain Sizing, Packaging Study, Thermal Simulation, Modal/Vibration Analysis, Homologation, AIS Standards, Energy Management Strategy.*

1. Introduction

1.1. What is a REEV?

A Range-Extended Electric Vehicle (REEV) is a battery-electric vehicle augmented with a small internal combustion engine and generator set that recharges the battery in operation rather than driving the wheels directly. Power flows from the IC engine and generator into the battery pack and subsequently to an Electric Drive Unit (EDU) that provides tractive power at the wheels. This architecture decouples the engine operating point from instantaneous road load, allowing the ICE to run at, or near, its most efficient point while the electric drivetrain manages transient torque demand. By extending the usable range beyond pure battery capacity, this configuration directly mitigates range anxiety in markets lacking robust charging infrastructure.

1.2. Motivation and Objective

As original equipment manufacturers (OEMs) explore REEV architectures to address range anxiety in markets with limited charging infrastructure, there is a need for a structured methodology to translate benchmark data and performance targets into a physically realizable, homologation-compliant chassis layout. The objective of this study is to propose three candidate chassis layouts: front-wheel drive (FWD), rear-wheel drive (RWD), and all-wheel drive (AWD) for a REEV platform and to converge on a preferred baseline through iterative packaging, thermal, vibrational, and regulatory analysis.

2. REEV Benchmarking

Twelve REEV models currently in production or nearproduction were identified and benchmarked, including the Li Auto L7/L9, Leapmotor C10, Voyah Free, BMW i3 REx, BYD Yangwang U8L, ROX Adamas, Aito M9, Deepal S09, M-Hero 917, Deepal G318 and Chery Exeed Sterra ET. Twelve parameter categories were used for comparison: energy consumption, fuel consumption, pure EV range, total extended range, battery capacity, curb weight and gross vehicle weight, IC engine specification, fuel tank capacity, floor topology, traction motor output, dimensions, and seating capacity. Based on data availability and representativeness of the segment, three reference vehicles–the Li Auto L9, Aito M9, and Chery Exeed Sterra ETwere selected as the primary benchmarking set.

Feature / Parameter	Aito M9 (2025)	Li Auto L9 (2026)	Chery Exeed Sterra ET
Seats	6	6	5
Pure EV Range (CD)	290 km CLTC	420 km CLTC	200 km CLTC
Total Extended Range	1474 km CLTC	1650 km CLTC	1518 km CLTC
Battery Capacity	52 kWh (NMC)	72.7 kWh (NMC)	32 kWh
Curb Weight (kg)	2560	2755–2835	2180
GVW (kg)	3010	3435	2595
ICE Engine Specs	1.5L, 4-Cylinder Turbo	1.5L, 4-cylinder Turbo	1.5L, 4-cylinder Turbo
ICE Engine Power	112 kW	115 kW	115 kW
Fuel Tank Capacity	65L	65L	67L
Traction Motor Output	365 kW (Dual Motor AWD)	420 kW (Dual Motor AWD)	195 kW (Rear Wheel Drive)
Energy Consumption	~ 22 kWh/100km	~ 22.2 kWh/100km	~ 17.3 kWh/100km CLTC
Fuel Consumption [L/100km]	6.4	6.3 (When battery under 20%)	—
Dimensions (mm)	5230 × 1999 × 1800	5255 × 2000 × 1810	4955 × 1975 × 1698
Power to Weight (kW/kg)	0.142	0.148	0.089
Steering Type	Rack & Pinion	Steer by Wire	Rack & Pinion
Floor Topology Retention	Skateboard	Skateboard	Skateboard

Figure 1: Benchmark comparison of reference REEV platforms

3. Methodology

3.1. Powertrain Sizing Formulation

Powertrain sizing was performed in two stages of fidelity. A standard spreadsheet-based tool computed cruise-mode power requirements from target range, acceleration time and maximum velocity inputs. A detailed MATLAB-based tool extended this with full driving-cycle simulation and regenerative braking modelling, producing battery capacity, fuel tank capacity, engine power and motor power as outputs.

3.2. Powertrain Sizing Governing Equations

Vehicle acceleration performance dictates the power required to take a vehicle of gross vehicle weight (GVW) mass m from rest to a final target velocity V_f within a specified time interval t_a. This is derived directly from $P = F \cdot v$, $F = m \cdot a$, and $a = dv/dt$:

$$P_{acc} = \frac{1}{\eta_t}\left(\frac{mV_f^2}{t_a}\right) \tag{1}$$

The peak power requirement at maximum velocity v_{max} encompasses rolling resistance, aerodynamic drag, and gradeability, converted with the appropriate unit-scaling constants:

$$P_{v_{max}} = \frac{1}{\eta_t}\left(\frac{mgfv_{max}}{3600} + \frac{mgiv_{max}}{3600} + \frac{C_D A(v_{max})^3}{76140}\right) \tag{2}$$

Similarly, the standard cruise power demand required to maintain a constant operating velocity v is given by:

$$P_{cruise} = \frac{1}{\eta_t}\left(\frac{mgfv}{3600} + \frac{mgiv}{3600} + \frac{C_D A v^3}{76140}\right) \tag{3}$$

The total system tractive demand placed on the engine additionally factors in secondary auxiliary loads such as HVAC, onboard electronics, and steering pumps:

$$P_{engine} = P_{cruise} + P_{auxiliary} \tag{4}$$

The volume of fuel required to cover the range-extending portion of the trip:

$$V_{fuel} = (R_{total} - R_{EV}) \times F_c \tag{5}$$

where the fuel consumption factor F_c is itself a function of average energy consumption, specific fuel energy density, and the combined thermal efficiencies of the IC engine and generator:

$$F_c = \frac{E_c}{\rho_{Ex} \times \eta_{eng} \times \eta_{gen}} \tag{6}$$

Finally, the benchmark energy consumption E_c used in Eq.6 is evaluated at a standardized highway cruise speed of 100 km/h using the cruise power expression of Eq.3:

$$E_c = P_{req} \times 1 = \text{Eq.3, with } v = 100 \text{ km/h} \tag{7}$$

where η_t is transmission efficiency, g is gravitational acceleration, f is the rolling resistance coefficient, i is the road gradient, C_D is the coefficient of aerodynamic drag, A is the vehicle frontal area, ρ_{Ex} is the specific energy density of the fuel, and η_{eng}, η_{gen} are the IC engine and generator efficiencies respectively.

3.3. Detailed MATLAB Drive-Cycle Simulation

The detailed sizing tool propagates vehicle input parameters through a WLTC Class 3b velocity profile, computes longitudinal dynamics and traction force at the wheel, and classifies the instantaneous power demand as motoring or regenerative braking. Motor and transmission losses or regenerative blending logic are applied before an energy calculation, range-extender analysis and fuel tank sizing step produce final outputs.

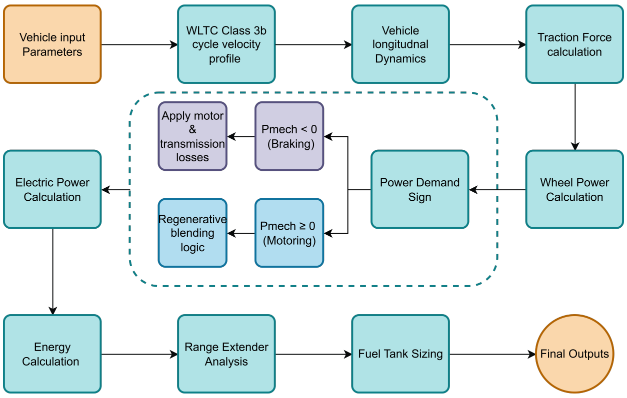

Figure 2: MATLAB simulation flow

Table 1: Simulation Results: Chery Exeed Sterra ET

Parameter	Benchmark Target	MATLAB Result
Energy utilization	21.1 kWh/100km	21.19 kWh/100km
Fuel Consumption	—	5.22 L/100km
Fuel Tank	67 L	64.93 Liters
Battery Capacity	32 kWh	38.62 kWh
Engine Power	115 kW	110.73 kW
Motor Power	195 kW	133.49 kW

Table 2: Simulation Results: Li Auto L9

Parameter	Benchmark Target	MATLAB Result
Energy utilization	22.2 kWh/100km	24.54 kWh/100km
Fuel Consumption	6.3 L/100km	6.05 L/100km
Fuel Tank	65 L	70.85 Liters
Battery Capacity	72.7 kWh	82.90 kWh
Engine Power	115 kW	101.73 kW
Motor Power	420 kW	260.05 kW

Table 3: Simulation Results: Aito M9

Parameter	Benchmark Target	MATLAB Result
Energy utilization	22.0 kWh/100km	23.05 kWh/100km
Fuel Consumption	6.4 L/100km	6.02 L/100km
Fuel Tank	65 L	67.21 Liters
Battery Capacity	52 kWh	58.11 kWh
Engine Power	112 kW	101.04 kW
Motor Power	365 kW	246.47 kW

3.4. Space Analysis and Component Sizing

3.4.1 Spatial Analysis and Component Scaling

While our initial parametric correlations provided a strong theoretical baseline, practical vehicle design must account for physical limitations. For example, arbitrarily increasing battery capacity to maximize range introduces unfeasible weight and packaging penalties. To address these constraints, we conducted a spatial analysis of the benchmarked vehicles. We extracted preliminary dimensions for key powertrain components by proportionally scaling chassis images, and subsequently refined this data for engineering accuracy through a detailed CAD review of existing vehicle architectures.

3.4.2 Development of Scaling Equations

Using these precise measurements, we developed empirical equations mapping component size to operational capacity. Similarly, by aggregating benchmark data, we formulated mass-scaling equations to accurately predict the weight impact of varying component sizes.

3.4.3 Powertrain Standardization and Optimization Formulation

Informed by benchmarking, we standardized the powertrain for our optimization model to a 1.5L, 4-cylinder turbocharged ICE (115 kW) and a 250 kW electric traction motor. Using these fixed parameters alongside established spatial and mass data, we formulated a mathematical optimization problem to determine the ideal energy storage configuration.

- **Objective Function:** Maximize total extended driving range.
- **Constraints:**
  - Meet the minimum pure EV range requirement.
  - Keep the total powertrain footprint within the maximum allowable chassis area.
- **Decision Variables (Outputs):** Optimal battery capacity and fuel tank volume.

Table 4: Sized vehicle vs. benchmark comparison

Feature / Parameter	**Our Car**	**Aito M9**	**Li Auto L9**	**Chery**
Pure EV Range (km)	200	240	345	164
Total Ext. Range (km)	1546	1200	1350	1245
Battery Capacity (kWh)	45 (LFP)	52 (NMC)	73 (NMC)	32 (LFP)
Curb Weight (kg)	2577	2560	2835	2180
ICE Engine	1.5L Turbo I4	1.5L Turbo I4	1.5L Turbo I4	1.5L Turbo I4
Fuel Tank (L)	70	65	65	67
Traction Motor (kW)	250	365 (AWD)	420 (AWD)	195 (RWD)

3.5. Lay-outing Approach

After finalizing powertrain specifications, we focused on spatial packaging, using the Li Auto L9's chassis as a geometric baseline due to similar component capacities. We developed preliminary layouts by analyzing benchmarked chassis imagery, validating these concepts through a detailed CAD review to resolve spatial conflicts. Finally, establishing fundamental frame dimensions and critical hardpoints allowed us to precisely position the primary powertrain components within the chassis envelope.

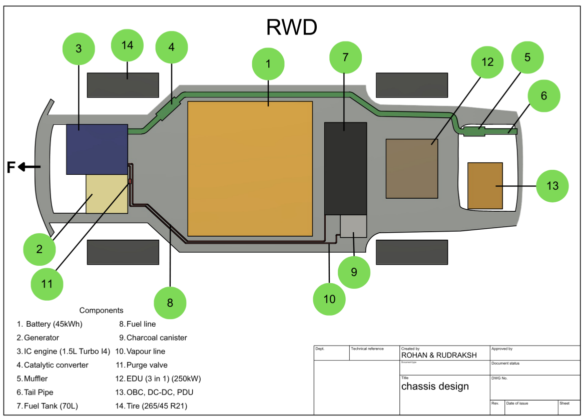

Figure 3: Chassis layout (First Iteration)

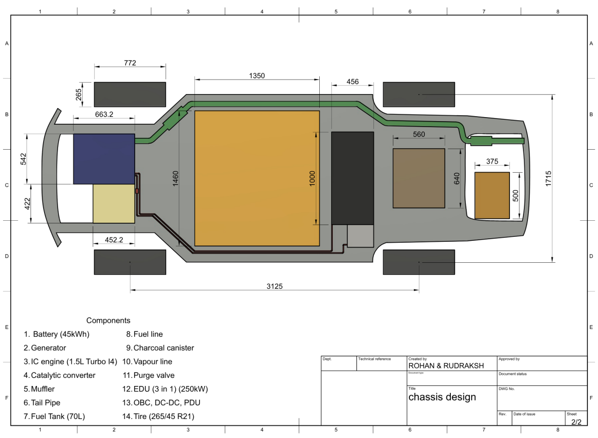

Figure 4: Chassis Layout Dimensions

3.6. Exhaust and Fuel System Architecture

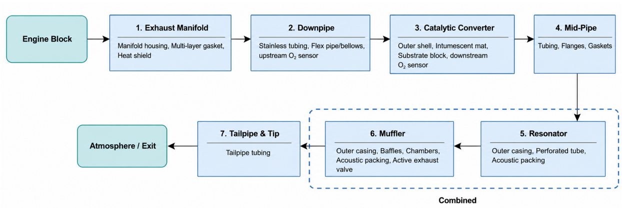

Figure 5: Exhaust System

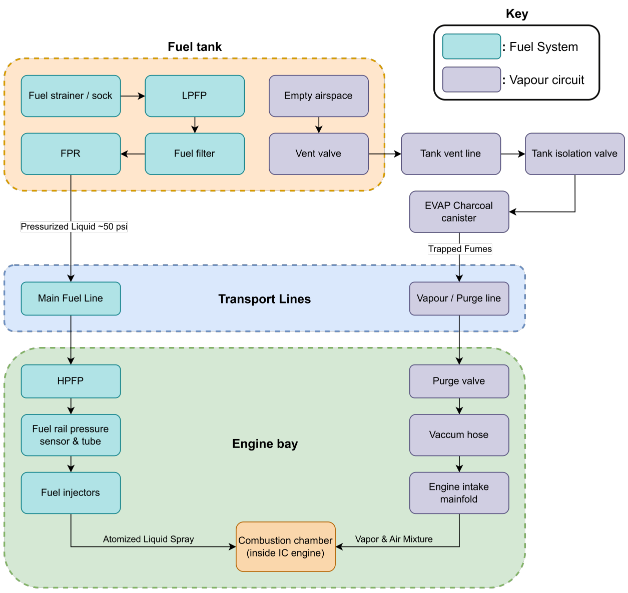

Figure 6: Fuel System and Vapour Circuit

3.6.1 EVAP Charcoal Canister Sizing

The ideal gas density of the fuel vapor, ρ_{vap}, is calculated using the atmospheric pressure P_{atm}, system temperature T, and the specific gas constant for the vapor R_{vap} (where $R_{\text{vap}} = 72.9$ J/(kg·K)):

$$\rho_{\text{vap}} = \frac{P_{\text{atm}}}{R_{\text{vap}} \cdot T} \tag{8}$$

The diurnal vapor mass generation, Δm_{vap}, is determined by the density differential between states and the predefined tank head volume ($V_{\text{head}} = 10.5$ L, representing 15% of the tank):

$$\Delta m_{\text{vap}} = (\rho_1 - \rho_2) \times V_{\text{head}} \tag{9}$$

To size the canister volume, V_{canister}, the system evaluates the diurnal mass generation against the expected number of EREV non-purge soak periods ($N_{\text{cycles, no-purge}}$), factoring in the carbon working capacity (WC) and the density of the active carbon (ρ_{AC}):

$$V_{\text{canister}} = \frac{\Delta m_{\text{vap}} \times N_{\text{cycles, no-purge}}}{WC \times \rho_{\text{AC}}} \tag{10}$$

Finally, the total mass of the carbon required, m_{carbon}, is derived directly from the vapor mass and the working capacity limit ($WC = 0.12$ g/g):

$$m_{\text{carbon}} = \frac{\Delta m_{\text{vap}}}{WC} \tag{11}$$

3.6.2 Returnless Low-Pressure Fuel Pump (LPFP) Sizing

The base fuel mass flow demand, $\dot{m}_f$ (in kg/s), is calculated using the engine power P_{eng} and the Brake Specific Fuel Consumption (BSFC ≈ 250 g/kWh):

$$\dot{m}_f = \frac{P_{\text{eng}} \times \text{BSFC}}{3.6 \times 10^9} \tag{12}$$

This mass flow is converted into a base volumetric flow, Q_{fuel}, utilizing the standard density of petrol ($\rho_{\text{fuel}} = 775$ kg/m^3):

$$Q_{\text{fuel}} = \frac{\dot{m}_f}{\rho_{\text{fuel}}} \tag{13}$$

To establish the operational target, a 10% prime design margin is applied to the volumetric flow to yield Q_{design}. Because this is a returnless system, the traditional 3× return factor is omitted, resulting in significantly lower overall pump flow demand:

$$Q_{\text{design}} = Q_{\text{fuel}} \times 1.10 \tag{14}$$

The required pump pressure differential, ΔP_{pump}, is the difference between the Fuel Pressure Regulator (FPR) outlet pressure ($P_{\text{out}} = 5$ bar) and the tank inlet pressure ($P_{\text{in}} \approx 0.3$ bar):

$$\Delta P_{\text{pump}} = P_{\text{out}} - P_{\text{in}} \tag{15}$$

The underlying hydraulic power, P_{hyd}, required to move the fluid is the direct product of the pressure differential and the design flow rate:

$$P_{\text{hyd}} = \Delta P_{\text{pump}} \times Q_{\text{design}} \tag{16}$$

Finally, the actual electrical power demand of the pump, P_{elec}, accounts for the mechanical pump efficiency ($\eta_{\text{pump}} = 0.35$) combined with an overarching 1.2 design safety margin:

$$P_{\text{elec}} = \frac{P_{\text{hyd}}}{\eta_{\text{pump}}} \times 1.2 \tag{17}$$

Table 5: Exhaust System Components and Materials

Component	Child Parts	Standard Material(s) Used
1. Exhaust Manifold	Manifold Housing	Cast Iron or Cast Stainless Steel
	Multi-layer Gasket	Multi-layer Steel (MLS)
	Heat Shield	Stamped Aluminium
2. Downpipe	Main Tubing	Stainless Steel
	Flex Pipe / Bellows	321 SS inner tube with 304 SS braided mesh
	O_2 Sensor	ZrO_2 in SS body
3. Catalytic Converter	Outer Shell	409 grade Stainless Steel
	Intumescent Mat	Ceramic fiber (alumina-silicate) & vermiculite
	Substrate Block	Cordierite (ceramic) or Metallic foil (coated in Pt/Pd/Rh)
	O_2 Sensor	ZrO_2 in SS body
4. Mid-Pipe	Main Tubing	409 grade SS
5. Resonator	Outer Casing & Perforated Tube	409 or 304 grade SS
	Acoustic Packing	Continuous filament Fiberglass or Stainless Steel wool
6. Muffler	Outer Casing & Baffles	409 Stainless Steel
	Acoustic Packing	Fiberglass or Basalt fiber
	Active Exhaust Valve	Cast SS housing with a Titanium/304 SS butterfly flap
7. Tailpipe	Tailpipe Tubing	409 grade Stainless Steel

Table 6: Fuel System Components and Materials

Component Group	Child Part	Standard Material(s)
Fuel Tank Section	Fuel Tank	High-Strength Stainless Steel or Multi-layer Plastic (HDPE + EVOH + Tie layers)
	Fuel Strainer / Sock	Nylon (Polyamide) or Polyester mesh
	LPFP & FPR	Housing: POM (Acetal) or PPS, Spring: Stainless Steel, Diaphragm: FKM
	Fuel Filter	Cellulose paper or Microglass fibers
Transport Lines	Flexible Lines (Main & Vapour)	Inner: FKM or ETFE, Middle: EVOH or PA12, Outer: PA12 or PA11
	Rigid Hard Lines	Aluminized Steel or Nylon-coated Steel
Vapour Circuit	EVAP Charcoal Canister	Housing: PA66 or PP, Active Material: Activated Carbon
	Vent Line & Isolation Valve	Housing: PA66-GF30, Plunger: Stainless Steel, Seals: FKM or Fluorosilicone
Engine Bay	High-Pressure Fuel Pump (HPFP)	Forged Stainless/High-Carbon Steel (often with DLC coatings)
	Fuel Rail & Pressure Sensor	Rail: Brazed Stainless Steel or Aluminum 6061-T6, Sensor Housing: Brass or Stainless Steel
	Fuel Injectors	Body: Stainless Steel, Nozzle: Hardened High-Alloy Steel
	Purge Valve	Housing: PA66-GF30, Seals: FKM
	Vacuum Hose	EPDM rubber or Silicone
	Engine Intake Manifold	PA66-GF35 (35% Glass-Fiber Reinforced PA66)

3.7. Hand Formulation of Exhaust Gas Temperature Decay

With component dimensions finalized, the next critical objective was determining their precise relative spatial arrangement. Beyond the physical structural constraints of the chassis, a rigorous thermal analysis was essential to evaluate component thermal interactions and optimize the exhaust system routing. To predict the temperature distribution along the length of the exhaust pipe, a first-principles, one-dimensional, steady-state thermal model was formulated. The convective heat transfer between the internal exhaust gas and the pipe wall, coupled with the combined convective and radiative heat losses from the exterior pipe wall to the ambient environment, are governed by:

$$\frac{dT_{gas}}{dx} = -\frac{h_{in}\pi D_i}{\dot{m}c_p}\left(T_{gas} - T_{wall}\right) \tag{18}$$

$$Q_{in} = h_{out}\pi D_o(T_{wall} - T_{amb}) + \epsilon\sigma\pi D_o\left(T_{wall}^4 - T_{amb}^4\right) \tag{19}$$

where T_{gas} and T_{wall} are the local gas and pipe-wall temperatures, T_{amb} is ambient temperature, h_{in} and h_{out} are the internal and external convection coefficients, D_i and D_o are the inner and outer pipe diameters, $\dot{m}$ is the exhaust mass flow rate, c_p is specific heat capacity, ϵ is surface emissivity, and σ is the Stefan–Boltzmann constant.

3.8. Thermal Simulation (ANSYS Icepack)

A CAD model was prepared of a 119-cell-series battery pack (116 Ah, 3.2 V per cell) of 45 kWh positioned adjacent to the fuel tank and generator along with exhaust running down the chassis. The car is assumed to be operating at its maximum capacity, and hence the Boundary conditions were specified as battery pack heat source of 850 W and a constant engine surface temperature of 100 °C; cold plates were modelled with Glycol-50 coolant at 0.2 kg/s (side) and 0.1 kg/s (bottom) with constant-pressure outlets which adds to 25LPM of coolant flow rate; the exhaust inlet condition was 30 m/s at 800 °C with a constant-pressure outlet, with additional heat-up from the catalytic converter.

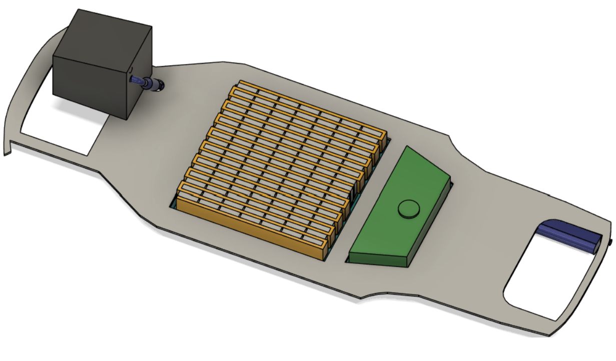

Figure 7: CAD Model

Initial thermal analysis revealed that the battery cell temperature reached 63°C and the fuel tank surface temperature peaked at 120°C. As both values significantly exceeded acceptable operational thresholds, critical design interventions were required. To mitigate these thermal loads, a perforated aluminum heat shield was integrated aft of the engine bay at the firewall, alongside the implementation of dedicated thermal encapsulation for both the battery pack and the fuel tank.

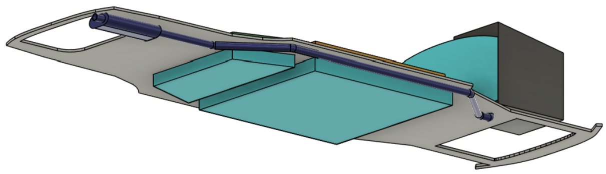

Figure 8: Updated CAD Model

3.9. Powertrain and Exhaust Mounting – Vibrational Analysis

Static components (battery, fuel tank, EDU) are rigidly mounted to the chassis, while dynamic components (engine, exhaust) require rubber isolators to prevent rotating-crankshaft and high-velocity exhaust-gas vibration from transferring into the passenger cabin. A modal analysis was conducted to determine optimal mount/hanger locations and the directional stiffness required of each isolator, with iterative tuning used to avoid resonance within known excitation bands.

The undamped equation of motion defines the dynamic equilibrium of the powertrain:

$$[M]\{\ddot{x}\} + [K]\{x\} = \{0\} \tag{20}$$

The global mass matrix $[M]$ combines the total mass m and inertia I at the center of gravity (CG):

$$[M] = \begin{bmatrix} m & 0 & 0 & 0 & 0 & 0 \\ 0 & m & 0 & 0 & 0 & 0 \\ 0 & 0 & m & 0 & 0 & 0 \\ 0 & 0 & 0 & I_{xx} & I_{xy} & I_{xz} \\ 0 & 0 & 0 & I_{yx} & I_{yy} & I_{yz} \\ 0 & 0 & 0 & I_{zx} & I_{zy} & I_{zz} \end{bmatrix} \tag{21}$$

The skew-symmetric matrix $[\tilde{r}_i]$ converts mount distances to rotational moments:

$$[\tilde{r}_i] = \begin{bmatrix} 0 & -z_i & y_i \\ z_i & 0 & -x_i \\ -y_i & x_i & 0 \end{bmatrix} \tag{22}$$

The global stiffness matrix $[K]$ aggregates the stiffness of all N mounts:

$$[K] = \sum_{i=1}^{N} \begin{bmatrix} [k_i] & [k_i][\tilde{r}_i]^T \\ [\tilde{r}_i][k_i] & [\tilde{r}_i][k_i][\tilde{r}_i]^T \end{bmatrix} \tag{23}$$

The eigenvalue problem serves as the core calculation to find the natural modes:

$$\det([K] - \omega^2[M]) = 0 \tag{24}$$

Finally, the natural frequency f_n converts the circular frequency to Hertz:

$$f_n = \frac{\omega_n}{2\pi} \tag{25}$$

Building upon this mathematical framework, we developed a computational tool designed to calculate the powertrain's modal frequencies using the system mass and 3x3 inertia matrix as primary inputs. By evaluating these outputs against target frequency bands, the tool enabled an iterative optimization process. This allowed us to precisely tune the mount coordinates and directional stiffness values to ensure optimal vibration isolation.

To validate our mathematical tool, we performed an ANSYS modal analysis on the exhaust system. Based on literature recommendations, we iteratively tuned mount locations and directional stiffness values to ensure the system's modal frequencies fell within the safe 10–25 Hz band, preventing resonance from external excitations. These optimized parameters were then used as inputs for our mathematical model, and the resulting modal frequencies were compared against the ANSYS outputs for validation.

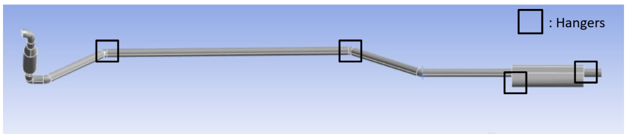

Figure 9: exhaust system hanger loactions

4. Results and Discussion

4.1. Finalised Chassis Components

Table 7: Comprehensive Vehicle and Auxiliary Specifications

Feature / Component Parameter	Value (Our Car)
Pure EV Range (km)	200
Total Ext. Range (km)	1546
Battery Capacity (kWh)	45 (LFP)
Curb Weight (kg)	2577
ICE Engine	1.5L Turbo I4
Fuel Tank (L)	70
Traction Motor (kW)	250
EVAP Charcoal Canister Capacity	~4 L
Fuel Pump Power	~36 W
Fuel Tank Wall Thickness	5 mm
Exhaust Pipe Internal Diameter	47.1 mm
Muffler Capacity	~15 L
Manifold Pipe Diameter	41 mm

4.2. Proposed Layout (First Iteration)

The first-iteration layout adopted a rear-wheel-drive (RWD) configuration, with the IC engine, generator and catalytic converter placed at the front, the battery pack occupying the central floor (skateboard) area, and the EDU, OBC/DC-DC/PDU module and muffler/tailpipe placed at the rear ahead of the rear axle. RWD was selected at this stage for easier packaging, balanced weight distribution, and future modularity/scalability of the platform.

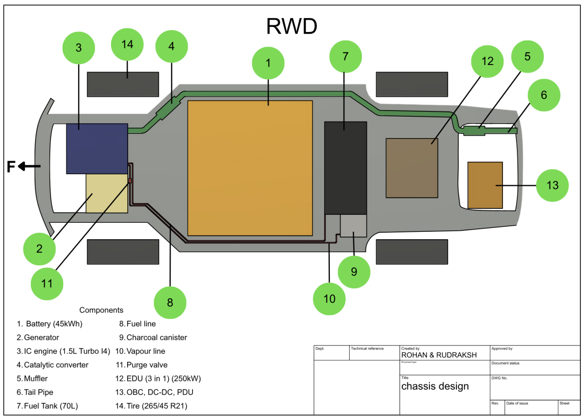

Figure 10: Chassis layout (First Iteration)

4.3. Thermal Simulation Results

Without any protective shielding, the simulation showed a peak cell temperature of 64.51 °C (exceeding the 60 °C absolute maximum limit) and a fuel tank (HDPE) body temperature of 119.04 °C, well above the 95 °C allowable limit – driven primarily by radiative and convective heating from the adjacent exhaust and engine bay.

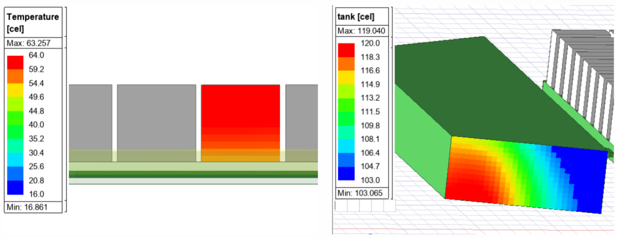

Figure 11: Results (without shields)

Introducing dedicated heat shields around the exhaust routing, battery pack, and fuel tank substantially reduced thermal loading.

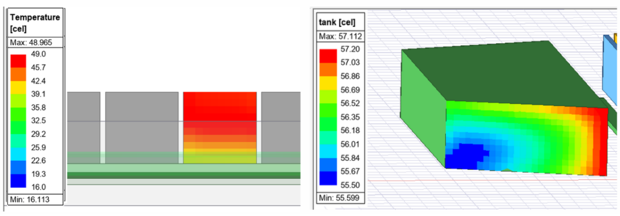

Figure 12: Updated Results (with shields)

Table 8: Thermal results comparison against allowable limits

Quantity	Limit	No Shield	With Shield	Hand Calc.
Cell Temp. (°C)	$<$ 45 long life $<$ 60 maximum	64.51	48.965	—
Base Coolant Temp. (°C)	45	51.18	38.413	—
Exhaust Outlet Temp. (°C)	300	292	313	280.12
Fuel Tank Body Temp. (°C)	95	119.04	57.12	—

With shielding in place, cell temperature, base coolant temperature and fuel tank temperature all fall within allowable limits. The exhaust outlet temperature rises slightly with shielding (313 °C vs. 292 °C without) due to reduced heat rejection along the pipe run, but remains within the 300–313 °C band consistent with the independent hand-formulation estimate of 280.12 °C, providing cross-validation between the CFD and analytical approaches.

4.4. Vibration Analysis of the Exhaust System

Modal analysis of the exhaust system with hangers positioned as shown in Fig.13 produced six resonance modes, compared in Table 9 against the analytical math model. Both approaches agree closely and fall within the required 10–25 Hz excitation-avoidance range.

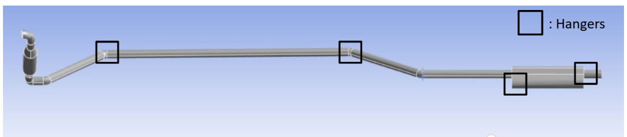

Figure 13: Exhaust system hanger locations

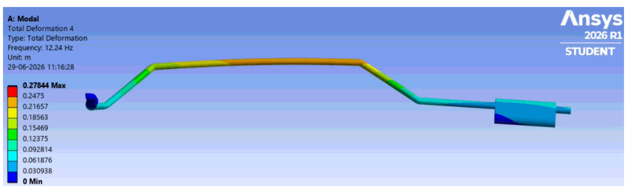

Figure 14: Exhaust system modal analysis

Table 9: Comparison of Resonance Frequencies

Mode	Resonance Frequencies (Hz)	
	FEA	Math Model
1	10.39	10.241
2	10.52	10.402
3	11.17	10.974
4	12.24	12.143
5	14.16	14.091
6	16.31	16.258

4.5. Final Layout

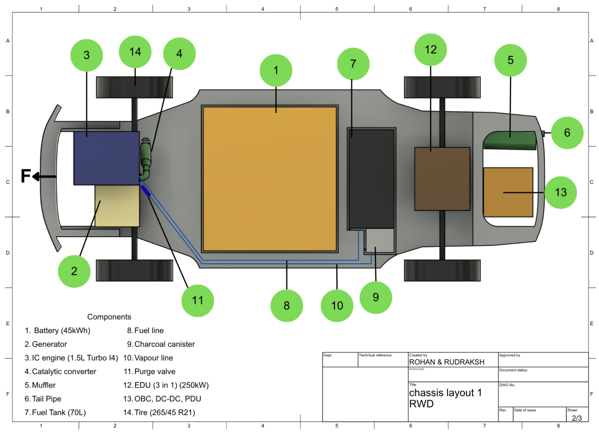

Figure 15: Final packaging RWD

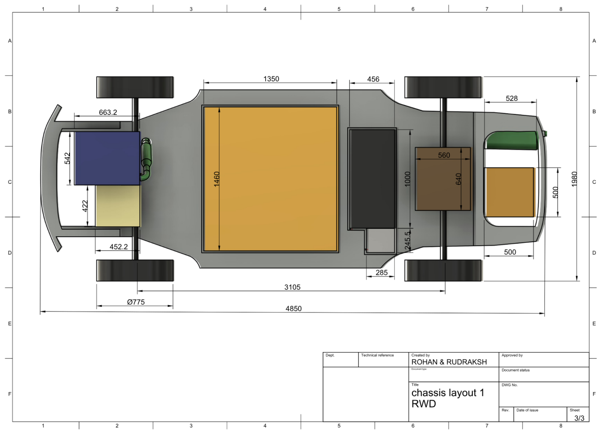

Figure 16: Final packaging RWD (dimensions)

5. Standards Analysis and Homologation

An automotive standards equivalency lookup was built mapping Indian AIS standards to their international counterparts (ISO, ECE, SAE/FMVSS, GB, JASO/JIS), illustrated for AIS-040 (fuel consumption declaration). A structured homologation review was then conducted across four domains: structural safety, high-voltage architecture, emissions/ICE type approval (BS-VI/AIS-137), and performance/thermal compliance.

Table 10: Homologation compliance summary against AIS standards

System	AIS Standard	Requirement	Current Design & Action	Status
1. STRUCTURAL SAFETY				
System	**AIS Standard**	**Requirement**	**Current Design & Action**	**Status**
Fuel Tank Placement	AIS-101	Tank must sit forward of rear sub-frame, outside all rear crush zones	The fuel tank is in front of the rear axle in our design	✓ Compliant
Underbody / Battery Shielding	AIS-048 / AIS-156	IPX7 waterproofing + directional gas venting for thermal runaway	IPX7 protection required in manufacturing	Action
Tank Overpressure	AIS-095	Dedicated expansion headspace in tank to prevent over-pressurisation	15% expansion volume is considered	✓ Compliant
Frontal Impact	AIS-098	HV/fuel systems must not be compromised in 56 km/h ODB frontal test	Front bay has structural reinforcement to prevent crush zone from reaching IC engine and generator	✓ Compliant
2. HIGH-VOLTAGE ARCHITECTURE				
System	**AIS Standard**	**Requirement**	**Current Design & Action**	**Status**
Dual-Mode Energy Logging	AIS-102	Architecture must log EV and REEV energy separately for OBD-II compliance	DP+NN controller tracks SOC and engine power history	✓ Compliant
Battery Pack Safety	AIS-156	Thermal runaway containment; cell-level BMS monitoring; isolation	119S cells, 45 kWh; max cell temp 48.97°C with shields	✓ Compliant
3. EMISSIONS & ICE TYPE APPROVAL (BS-VI / AIS-137)				
System	**AIS Standard**	**Requirement**	**Current Design & Action**	**Status**
OBD-II Diagnostics	AIS-137 Annex	Emission-related DTCs and freeze-frame data required during CS mode	NN controller tracks engine power; no OBD specifications yet. Specify OBD-II compliant ECU; map diagnostic trouble codes to AIS-137 Annex	Action
EVAP System	AIS-031 / CMVR R.115	Charcoal canister must adsorb fuel vapours; purge during engine-on phases	Did charcoal canister sizing; incorporated purge valve to engine intake in our design	✓ Compliant
Exhaust Heat & Surface Temp	AIS-056	Exhaust surface temp near fuel/brake lines within safe limits; heat shields mandated	Did thermal simulations for the exhaust and validated the results	✓ Compliant
Fuel Consumption Declaration	AIS-040	Official L/100 km (CS) and EV range (km) must be declared for type approval	MATLAB simulation result: 5.22 L/100 km	✓ Compliant
4. PERFORMANCE & THERMAL				
System	**AIS Standard**	**Requirement**	**Current Design & Action**	**Status**
Coolant Line Routing	AIS-082	High-pressure lines with generous bend radii; no flow restriction at max heat rejection	Glycol 50: 0.2 kg/s side plates, 0.1 kg/s bottom plates. Modified the cold plate lines with bend radius 3× pipe OD	✓ Compliant
Fuel Tank Temperature	AIS-095	HDPE tank body temperature must stay below 95°C	Thermal simulation (with shields): max 57.12°C – within limit	✓ Compliant

6. IC Engine and Generator Operating Strategy

6.1. Energy Management Strategy

The Energy Management System (EMS) supervises the operation of the engine, generator, battery and traction motor. The primary objective is to minimize fuel consumption while maintaining the battery SOC within predefined limits.

Energy management strategies are broadly classified as Rule-Based Control: Deterministic Rule-Based and Fuzzy Logic Rule-Based or Optimization-Based Control: Global Optimization and Instantaneous Optimization

Rule-based strategies are computationally efficient but are dependent on manually designed rules. Optimization-based approaches provide globally optimal solutions but are computationally intensive. Therefore, a hybrid framework combining offline optimization and online learning is adopted.

6.2. Proposed Hybrid Strategy

The proposed energy management framework consists of

1. Offline Dynamic Programming
2. Online Neural Network Controller

Dynamic Programming generates globally optimal engine operating decisions over representative drive cycles. These optimal trajectories are used to train a neural network that predicts engine power in real time.

7. Methodology

7.1. Phase I: Power Demand Calculation

Vehicle power demand is calculated using

$$F_{tr} = F_{roll} + F_{aero} + F_{grade} + F_{acc} \tag{26}$$

where

$$F_{roll} = mgC_{rr} \tag{27}$$

$$F_{aero} = \frac{1}{2}\rho C_d A v^2 \tag{28}$$

$$F_{grade} = mg\sin\theta \tag{29}$$

$$F_{acc} = ma \tag{30}$$

The required power is

$$P_{req} = F_{tr}v \tag{31}$$

7.2. Phase II: Dynamic Programming Optimization

Dynamic Programming minimizes

$$J = \sum_{k=1}^{N} \left(Fuel_k + \lambda(SOC_k - SOC_{target})^2\right) \tag{32}$$

subject to engine and battery operating constraints. The optimization produces optimal engine power, battery power and SOC trajectories.

7.3. Phase III: Neural Network Training

The DP dataset is used to train a Multilayer Perceptron (MLP). The network inputs include required power, vehicle speed, battery SOC, target SOC, driving mode, previous engine power and battery depletion rate.

The learned mapping is

$$P_{eng} = f(P_{req}, SOC, v, \text{Driving Mode}, \ldots) \tag{33}$$

Separate controllers are trained for different trip distances.

7.4. Phase IV: Online Controller

The required depletion rate is

$$E_{need} = \frac{SOC_{current} - SOC_{target}}{\text{Remaining Distance}} \tag{34}$$

The appropriate neural network predicts engine power in real time. A rate limiter is applied before sending commands to the engine-generator unit.

7.5. Phase V: Pulse Thermostat Operation

The engine is operated only at its highest efficiency operating point. Excess power charges the battery, after which the engine is turned off until the battery SOC reaches its lower threshold.

7.6. Phase VI: Performance Evaluation

The proposed controller is compared against conventional CD/CS control and Dynamic Programming using

- Fuel consumption
- Fuel economy
- Final SOC
- Fuel savings
- SOC tracking accuracy
- Engine operating point distribution
- Computational time

Table 11: Projected performance vs. CD/CS baseline

Parameter	**Our Model vs. CD/CS**
Strategy	Offline DP + Online NN
Fuel Consumption	~7–10% improvement
Battery Health	Better (avoids deep discharge, lower C-rate stress, shallower cycling depth)

8. Final 3 Layouts: FWD, RWD and AWD

Three concept layouts were developed and compared on packaging, weight distribution, cabling complexity and cost.

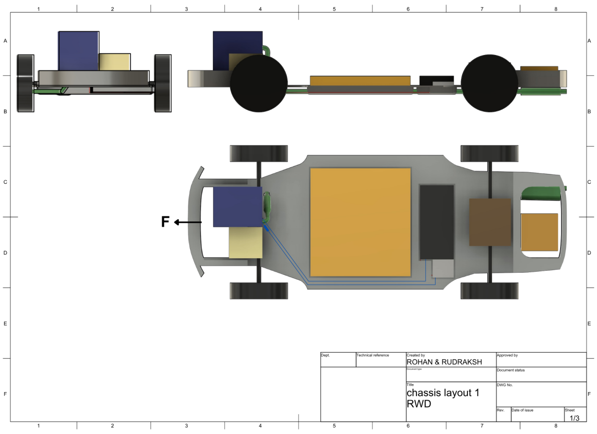

Figure 17: Concept Layout 1 (RWD): battery-centred skateboard with engine/generator front and EDU rear

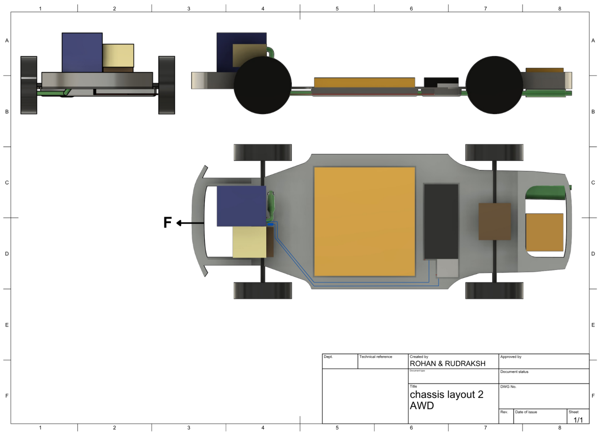

Figure 18: Concept Layout 2 (AWD): dual-motor configuration (150 kW rear, 100 kW front, front motor beneath the generator)

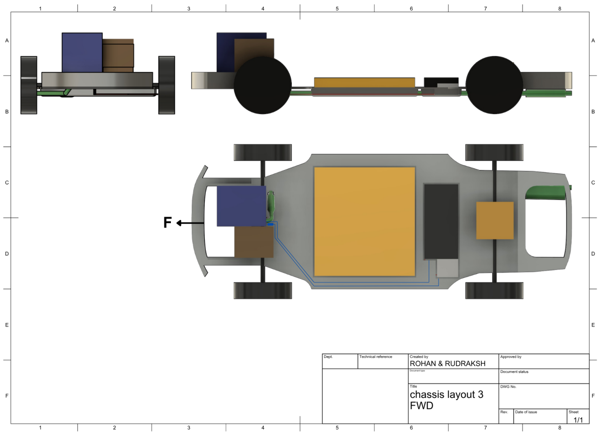

Figure 19: Concept Layout 3 (FWD): EDU relocated to the front axle with the 3-in-1 OBC/PDU/DC-DC module at the rear

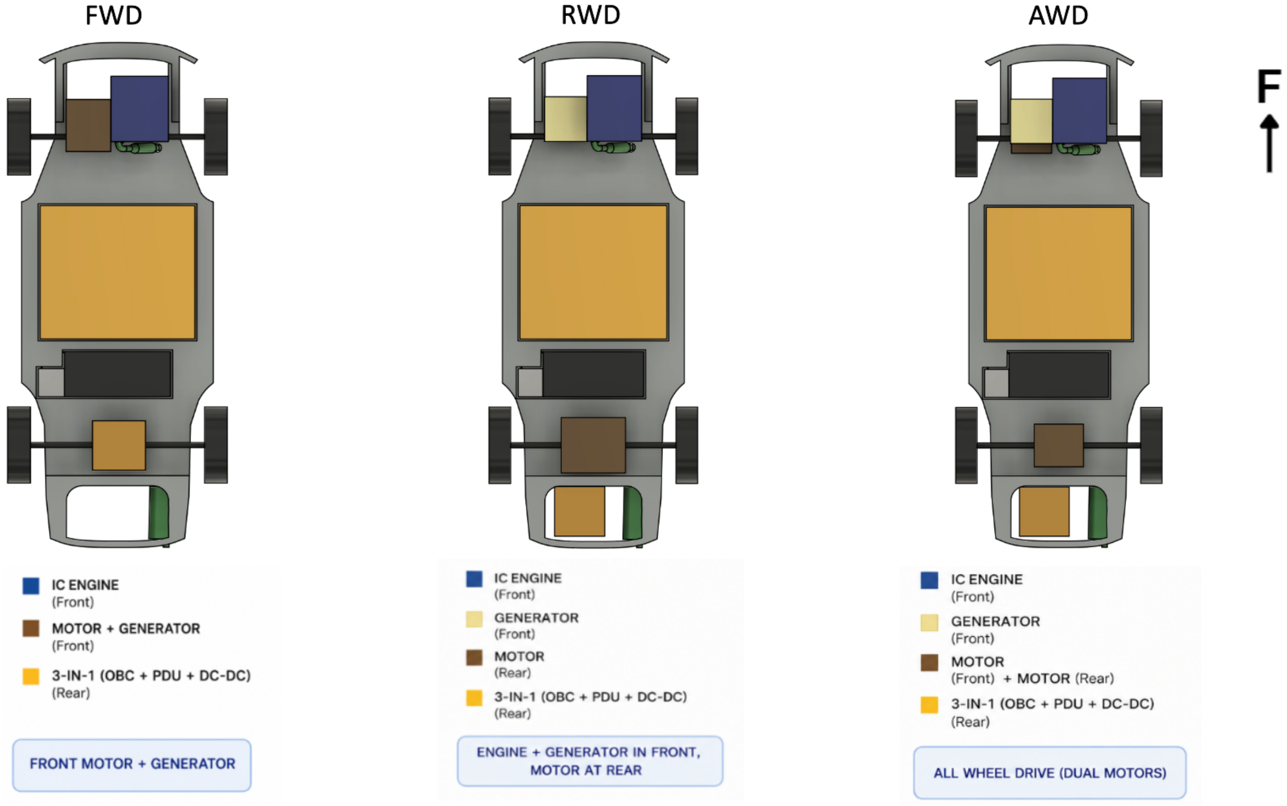

Figure 20: Comparison of FWD, RWD, and AWD powertrain layout concepts

Table 1: Comparison of Electric Drivetrain Architectures

	RWD (Rear-Wheel Drive)	**FWD (Front-Wheel Drive)**	**AWD (All-Wheel Drive)**
Pros	• Best weight distribution • Better traction under acceleration (rear weight transfer) • Less torque steer • Easier packaging	• Lowest cost • Completely free rear space • Shortest HV cabling hence fewest conversion losses	• Best traction and handling • Regen. braking on both axles hence highest energy recovery • Torque vectoring for better cornering/yaw control
Cons	• Long HV cable hence losses and complex routing • Less cargo/spare space • Poor weather traction • Poor regenerative braking	• All traction on front tires so understeer and front tire wear • Poor weight distribution • Tight front packaging limits motor torque ceiling • Poor regenerative braking	• Highest cost (two motors, two inverters) • Most complex thermal/control system across two zones

Weighing packaging simplicity, weight balance, and platform scalability against cost and control complexity, the RWD configuration was retained as the baseline production-intent layout, with AWD identified as a premium/performance derivative for future scope.

9. Conclusion

This study demonstrates an end-to-end modular platform layout methodology for a REEV chassis, beginning with benchmarking of twelve reference vehicles and progressing through powertrain sizing, packaging, exhaust/fuel system design, thermal simulation, vibrational analysis and regulatory homologation review. The sized vehicle achieves a 200 km pure-EV range and 1546 km total extended range using a 45 kWh LFP battery, a 1.5 L turbocharged four-cylinder engine and a 250 kW traction motor. Thermal simulation confirmed that unshielded battery and fuel-tank temperatures exceed AIS allowable limits, and that the introduction of heat shields brings all monitored quantities within limits, with the exhaust outlet temperature cross-validated between CFD simulation (313 °C) and an independent hand formulation (280.12 °C). Modal analysis confirmed that the exhaust hanger design avoids resonance within the required 10–25 Hz band. A structured homologation review found the design largely compliant with AIS structural, high-voltage, emissions and thermal requirements, with two action items remaining around IPX7 underbody sealing and OBD-II diagnostic specification. Of the three concept layouts developed (FWD, RWD, AWD), the RWD configuration was selected as the preferred baseline for its balance of packaging simplicity, weight distribution and cost.

10. Limitations and Future Scope

10.1. Limitations of IC engine operating strategy

- **Complex integration:** offline DP and online NN control layers may be difficult to integrate without instability or energy loss.
- **Real-time constraints:** the NN controller must execute quickly on production hardware, which becomes harder as model size grows.
- **Simulation-only validation:** most performance and thermal results are derived from simulation; real-world vehicle testing is required to confirm generalisation and reliability.

10.2. Future Outlook of the Strategy

- Improve interpretability and safety assurance by adding transparent decision logic and safety constraints so certifying authorities can trust NN outputs.
- Close the real-world validation gap by combining simulation with physical vehicle testing.
- Pursue emerging-technology convergence, including digital twins for aging tracking/recalibration and solid-state batteries (projected 15–20% reduction in aging).

10.3. Future Scope of Work

- **Complete vehicle integration:** finalise HV cable and coolant line routing, package remaining electrical components (VCU, PDU, sensors), and optimise suspension integration/accessibility.
- **Structural validation:** develop a detailed CAD chassis model, perform chassis stiffness analysis, validate mount strength for key components, and run frontal/side/rear crashworthiness simulations.
- **Detailed thermal analysis and design:** cooling-loop design for battery, motor and engine; underbody airflow optimisation; radiator and heat-rejection study.
- **IC engine operation strategy:** refine the proposed model for real-life implementation, study hardware integration requirements, and validate the strategy at full-vehicle level.

References

[1] REEV Benchmarking dataset (internal spreadsheet, REEV.xlsx), 2026.

[2] Standards equivalency dataset (internal spreadsheet, Standards.xlsx), 2026.

[3] Benchmarked vehicle chassis reference imagery, internal design repository, 2026.

[4] "Review of Range-Extended Electric Vehicle Powertrain Architectures and Control Strategies," *SAGE Journals*, DOI: 10.1177/16878132221149890.

[5] Automotive Industry Standard (AIS) compliance summary, internal documement, 2026.

[6] B. Huang, W. Yu, M. Ma, X. Wei, and G. Wang, "Artificial-Intelligence-Based Energy Management Strategies for Hybrid Electric Vehicles: A Comprehensive Review," Energies, vol. 18, no. 14, p. 3600, 2025, doi: 10.3390/en18143600.

[7] E. M. Szumska, "Regenerative Braking Systems in Electric Vehicles: A Comprehensive Review of Design, Control Strategies, and Efficiency Challenges," Energies, vol. 18, no. 10, p. 2422, 2025, doi: 10.3390/en18102422.

[8] X. Wang, S. Liu, P. Ye, Y. Zhu, Y. Yuan, and L. Chen, "Study of a Hybrid Vehicle Powertrain Parameter Matching Design Based on the Combination of Orthogonal Test and Cruise Software," Sustainability, vol. 15, no. 14, p. 10774, 2023, doi: 10.3390/su151410774.

[9] L. Xi, X. Zhang, C. Sun, Z. Wang, X. Hou, and J. Zhang, "Intelligent Energy Management Control for Extended Range Electric Vehicles Based on Dynamic Programming and Neural Network," Energies, vol. 10, no. 11, p. 1871, 2017, doi: 10.3390/en10111871.

[10] Y. Yang, Y. Xu, H. Zhang, F. Yang, J. Ren, X. Wang, P. Jin, and D. Huang, "Research on the energy management strategy of extended range electric vehicles based on a hybrid energy storage system," Energy Reports, 2022, doi: 10.1016/j.egyr.2022.05.013.

[11] Shashank.N, Shashank.P, and Gopalakrishna.HD, "Design and Analysis of Skateboard Electric Vehicle Chassis and Battery Pack," International Journal of Engineering Research & Technology (IJERT), vol. 12, no. 8, Aug. 2023.

[12] C. Musardo, G. Rizzoni, Y. Guezennec, and B. Staccia, "A-ECMS: An Adaptive Algorithm for Hybrid Electric Vehicle Energy Management," European Journal of Control, vol. 11, no. 4-5, pp. 509–524, 2005, doi: 10.3166/ejc.11.509-524.

[13] W. Faris, "Automotive Noise, Vibration, and Harshness (NVH): A Thematic Literature Review," Vehicles, vol. 8, no. 6, p. 140, 2026, doi: 10.3390/vehicles8060140.

[14] S. Ahmed, H. Rottengruber, and M. Full, "Hybrid model for exhaust systems in vehicle thermal management simulations," Automotive and Engine Technology, vol. 7, no. 1-2, pp. 115–136, 2022, doi: 10.1007/s41104-022-00104-w.

[15] Xiao, Shenghao & Cheng, Si. (2023). Research on noise control of automobile exhaust system under idling condition based on modal analysis. Advances in Mechanical Engineering. 15. 168781322211498. 10.1177/16878132221149890.